Applied Catalysis B: Environmental 312 (2022) 121367

Contents lists available at ScienceDirect

Applied Catalysis B: Environmental

journal homepage: www.elsevier.com/locate/apcatb

Flexo-phototronic effect in centro-symmetric $BiVO_4$ epitaxial films

Pao-Wen Shao [a,b], Meng-Chin Lin [c,d], Qian Zhuang [e,f], Jiawei Huang [e,f], Shi Liu [e,f,g], Hsiao-Wen Chen [h], Hsiang-Lin Liu [h], Yu-Jung Lu [b], Yung-Jung Hsu [a], Jyh-Ming Wu [c,d], Yi-Chun Chen [i], Ying-Hao Chu [a,c,*]

[a] Department of Materials Science and Engineering, National Yang Ming Chiao Tung University, Hsinchu 30010, Taiwan
[b] Research Center for Applied Sciences, Academia Sinica, Taipei 11529, Taiwan
[c] Department of Materials Science and Engineering, National Tsing Hua University, Hsinchu 30013, Taiwan
[d] High Entropy Materials Center, National Tsing Hua University, Hsinchu 30013, Taiwan
[e] School of Science, Westlake University, Hangzhou, Zhejiang 310024, China
[f] Institute of Natural Sciences, Westlake Institute for Advanced Study, Hangzhou, Zhejiang 310024, China
[g] Key Laboratory for Quantum Materials of Zhejiang Province, Hangzhou, Zhejiang 310024, China
[h] Department of Physics, National Taiwan Normal University, Taipei, Taiwan
[i] Department of Physics, National Cheng Kung University, Tainan, Taiwan

ARTICLE INFO

Keywords:
Flexo-phototronic
Flexoelectricity
Strain gradient
Centro-symmetry
Domain wall

ABSTRACT

With exciting functionality, topological defects in ferroic system have attracted significant attention. Under proper design, the emergence of polar domain walls in non-polar ferroelastics enables a flexo-phototronic effect. In this study, we revealed ferroelastic twin texture with localized flexoelectric effect in centrosymmetric epitaxial $BiVO_4$ film. Supported by photodeposition and localized photocurrent analysis, we found the flexoelectric effect confined at domain wall area facilitates the photocarrier transport and the flexo-phototronic mechanism was further supported by dye-degradation and generation of reactive radicals. This work not only provides new insights into the introduction of flexo-phototronic effects in non-polar materials, but also sheds light on the use of material inhomogeneity for acquiring multifunctionality.

1. Introduction

Multifunctional materials are desirable for next-generation electronic devices. They can be obtained through an utilization of mutual coupling among various kinds of physical mechanisms [1]. For example, the piezo-phototronic effect is a coupling of piezoelectric, semiconductor and photonic behaviors [2–5]. Imposing a strain to generate a piezo-potential can be used to control carrier generation, transport, separation, and recombination in semiconductors for optoelectronic devices [6,7]. Typically, such an effect occurs in materials with a break of centrosymmetry, classified as polar materials, setting up a criterion for material selection [8]. However, inhomogeneity, such as topological defects, exists naturally in materials and can present symmetry and properties unlike bulk materials [9]. For example, polar domain walls are theoretically predicted [10,11] and experimentally observed [12] in centrosymmetric system, especially in ferroelastic system since energy equivalent structures endow inhomogeneity at domain walls. It turns out that the intrinsic flexo-electricity in ferroelastic domain walls can offer flexopotential, which is forbidden by symmetry in bulk, enhancing the feasibility to achieve flexo-phototronics in centrosymmetric photo-active system, which would be a giant improvement for photoelectrochemistry.

In this study, centrosymmetric $BiVO_4$ (BVO) is selected as a model system, because it is an attractive candidate for photoanode by virtue of its adequate bandgap (2.4–2.6 eV) and the advantages of non-toxicity and high stability [13]. Efforts on enhancing its photoelectrochemical performance were mostly focused on building up heterojunction for effective charge separation [14,15]. Besides, recent attention was paid to the control and utilization of material inhomogeneity for further improving its photo-activity. By virtue of ferroelastic characteristic of monoclinic BVO (I2/b, a=5.204 Å, b=5.101 Å, c=11.69 Å, $\gamma = 89.6°$), BVO is reported with surface polarity [16], manifesting polar domain

Abbreviations: BVO, $BiVO_4$; YSZ, yttria-stabilized zirconia; DFT, density functional theory; RhB, rhodamine B; EPR, electron paramagnetic resonance; DMPO, 5,5-dimethyl-1-pyrroline N-oxide; DMSO, dimethyl sulfoxide; FFT, fast Fourier transform.

* Corresponding author at: Department of Materials Science and Engineering, National Tsing Hua University, Hsinchu 30013, Taiwan.
E-mail address: yhchu@mx.nthu.edu.tw (Y.-H. Chu).

https://doi.org/10.1016/j.apcatb.2022.121367
Received 25 December 2021; Received in revised form 15 March 2022; Accepted 31 March 2022
Available online 8 April 2022

walls in centrosymmetric matrix, which is also observed in other ferroelastic system (e.g., $SrTiO_3$ [17]). In addition, the intrinsic flexoelectric-coupled photovoltaic effect [18] further suggests that the flexoelectricity of BVO plays an essential role in photoelectric conversion efficiency. Therefore, considering that flexoelectric BVO displays electromechanical coupling in analog to typical piezoelectric material, further speculation of applying flexoelectric BVO to piezo-catalytic energy conversion [19,20] remains an attracting research direction (e.g., converting mechanical energy into chemical one without light irradiation), and we anticipate it would expand the potential application of material inhomogeneity.

In this work, we fabricated epitaxial ferroelastic BVO films on yttria-stabilized zirconia (YSZ) substrate. The polar domain walls can be predicted by first-principles density functional theory (DFT) calculations and revealed by piezoresponse force microscopy. The mechanism of the flexopotential improved photoactivity is probed by photodeposition of Au nanoparticles and flexo-photo-degradation of rhodamine B (RhB). The importance of BVO domain patterns is highlighted by spatial-resolved photoconductivity and photochemistry. We found that the flexoelectricity at domain walls in centro-symmetric BVO creates a flexopotential to enhance photocatalytic performance. Our results not only lessen the gap on the development of piezo-based catalyst, but also launch a new research direction of flexo-phototronics.

2. Experimental details

2.1. Sample preparation

BVO epitaxial films were fabricated on YSZ substrate via pulsed laser deposition [21]. YSZ substrates were pre-annealed at 1300 ℃ for 8 h. The KrF excimer laser (λ = 248 nm, COMPex 102, Coherent) was operated at laser fluence of 1 J/cm^2 using commercial BVO target. The oxygen pressure was maintained at 60 mTorr and the deposition temperature was kept at 550 ℃. After the deposition, the cooling rate was 25 ℃/min.

2.2. Piezoresponse force microscopy and conductive atomic force microscopy

PFM results were collected by a commercial SPM system (Asylum Research MPF-3D) using commercial Platinum coating tips (mikromasch HQ:NSC36/PT, cantilever C, resonance frequency = 65 kHz). Figs. 1b-d and 4e were conducted at the in-plane contact resonance frequency (about 680 kHz) at DART mode with AC tip bias of 1.5 V. CAFM was performed on a commercial SPM system (Bruker MultiMode 8 SPM system) and the light source was 405 nm laser pointer. Gold commercial tips (Rocky Mountain 25PT400B) were used for photocurrent detection.

2.3. Photo deposition

$HAuCl_4$ was chosen for the precursor because the reduction potential of $HAuCl_4$ to Au is lower than the conduction band of BVO [22]. 40 μM $HAuCl_4$ was prepared for precursor, and the stirring speed was kept at 300 rpm. 20 μl ethanol was added as hole scavenger. BVO/YSZ sample was immersed in the precursor, perpendicular to the simulated light incident direction. The energy intensity of simulated light was 50 mW/cm^2 while the reaction time was 15 min. After the reaction, the sample was rinsed with deionized water and ultrasonic cleaner for 1 s

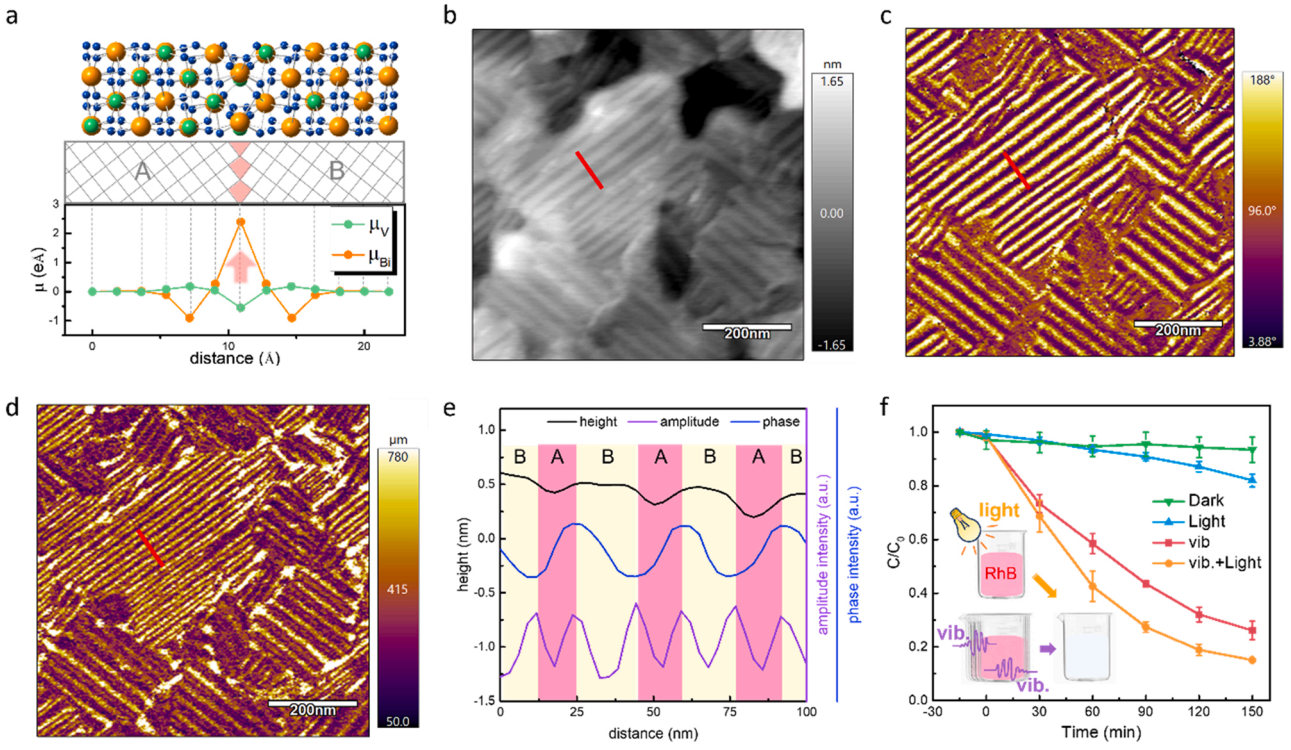

Fig. 1. (a) DFT calculations of ferroelastic BVO structures. Local electrical dipoles centered at V and Bi atoms across the supercell containing A/B domain wall. The red arrows represent the net polarization with respect to the center of their surrounding oxygen cages. The green, orange, and blue atoms represent V, Bi, and O atoms. (b) The topography of BVO/YSZ film. The according in-plane PFM (c) phase and (d) amplitude signal recorded simultaneously. (e) Line profile extracted from the red mark of (b, c) and (d), (f) Photo-degradation, flexo-degradation, and flexo-photo-degradation of RhB by BVO film, and they are represented by light, vibration, as well as light and vibration in the figure, respectively. Dark condition represents the absorption of RhB by catalyst based on the controlled dark condition without any stimuli.

2.4. Photodegradation

The $BiVO_4$ were mixed with the RhB solution (10 ppm) to evaluate their degradation activity. Before the degradation test, the absorption effect was evaluated by placing BVO sample in the dye solution under a dark environment for 15 min. Thereafter, the experiments were carried out under the three different conditions of light illumination (with a 150 W Xe lamp), ultrasonic vibration (at 300 W with 40 kHz) and applied light irradiation with simultaneous ultrasonic vibration to simulate photo-degradation, flexo-degradation, and flexo-photo-degradation, respectively. Degradation activity (i.e., concentration of RhB) was measured by absorption spectrum using an UV–vis photo-spectrometer (Hitachi, U3900).

2.5. Electron paramagnetic resonance spectroscopy

The reactive species created by the flexo-catalyst were detected by the electron paramagnetic resonance (EPR) technique with BRUKER E-580 spectrometer. First, a 0.5 * 0.5 cm^2 sample was placed in a bottle with 10 mL DI water and 1.2 mL 5,5-dimethyl-1-pyrroline N-oxide (DMPO) solution. After ultrasounds of 3, 10, 20 mins, the piezoelectrically generated •OH radicals were trapped by DMPO to form DMPO•-OH. For the $•O_2$- radicals detection, 1 mM DMPO in DMSO solution was prepared as the radical scavenger to form DMPO-$•O_2$. Under ultrasonic vibration for 3, 10, 20 min, the $•O_2$- created by the piezocatalyst was detected.

2.6. DFT calculations

First-principles DFT calculations were carried out using QUANTUM-ESPRESSO package [23] with PBEsol ultrasoft pseudopotentials taken from the Garrity, Bennet, Rabe, Vanderbilt high-throughput pseudopotential set [24]. The supercell containing two twin domain walls has 288 atoms. The cell dimensions are fixed to values determined based on optimized lattice constants of orthorhombic unit cell of BVO, following the same protocol in Ref. [25]. Given the large supercell size, the structure was optimized using a plane-wave cutoff of 40 Ry, a charge density cutoff of 200 Ry, a Marzari–Vanderbilt smearing of 1 mRy, and the Gamma-point algorithm. The atoms are fully relaxed until the force is below 1.0×10^{-4} Ry/Bohr.

3. Results and Discussion

3.1. Characterization and flexo-phototronics of BVO film

BVO exhibits ferroelasticity at room temperature with centro-symmetric space group I_2/b [26,27]. Detailed structural characteristic is shown in Fig. S1. One critical inhomogeneity of material, flexoelectric domain wall, can be expected. The properties of this inhomogeneity can be predicted by the first-principles density functional theory (DFT) calculations. We found that a spontaneous polarization arises at domain wall area, as depicted in Fig. 1a. In addition, Bi and V atoms at the interfaces between A/B domains are displaced appositively with respect to the center of their surrounding oxygen cages along the domain walls, respectively. (The detailed assumptions and quantified polarization are described in Fig. S2.) Such results indicate the possibility that inhomogeneity induces polarization in centrosymmetric materials [28–30].

In addition, the localized electromechanical coupling effect of BVO/YSZ thin film is revealed regardless of its centrosymmetric crystal structure. From piezoresponse force microscopy and twin domain morphology (Fig. 1b) recorded simultaneously, the in-plane PFM phase channel (Fig. 1c) gives information on the orientation of local electromechanical coupling, while the in-plane PFM amplitude channel (Fig. 1d) provides the magnitude of the lateral piezoresponse [31,32]. In order to rule out the artifact that the converse flexoelectric effect could be also induced by scanning tip, in which the magnitude of flexo-induced piezoresponse is a function of the applied force [33], we maintained the constant force and driving ac bias of the tip and it implies the resulting tip-induced piezoresponse remains constant during scanning. (The applied force is calculated to be ~30 nN in supplementary text S1.) Surprisingly, we obtained the in-plane domain distribution of BVO thin film (Fig. 1c, d). In addition, the red section lines were extracted to a profile diagram (Fig. 1e), which further combines the information of height, phase, and amplitude. It reveals that the domain distribution we observed is independent of topography, and the piezoresponse was only detected at domain walls rather than all domain areas (Fig. 1d), revealing the key role of these inhomogeneities and localized flexoelectric effect at domain walls. The reason why neighboring domain walls display the opposite contrast of phase signal could be explained by the difference of a and b parameters of BVO (monoclinic I2/b, a=5.204 Å, b=5.101 Å, c=11.69 Å, $\gamma = 89.6^\circ$). Considering the out of plane orientation relationship of BVO/YSZ (i.e., $[001]_{BVO}||[001]_{YSZ}$), the in-plane orientation could be $[100]_{BVO}||[100]_{YSZ}$ for A domains and $[010]_{BVO}||[100]_{YSZ}$ for B domains [34], and the opposite strain gradient could be expected between A-B and B-A domain walls. In addition, strain gradients results in flexoelectric effect. Therefore, the A-B-A-B sequence of domain distribution results in opposite directions of polarization, representing the head-to-head piezoresponse configuration at neighboring domain walls, which is also predicted in DFT calculations (Fig. S2). Furthermore, each domain wall generally displays the equivalent magnitude of amplitude, displaying the typically piezoelectric property of ferroelectrics, in which the amplitude value is expected to be equal for area with different phase contrast [35]. This result clearly demonstrates the piezoresponse concentrated at domain wall is ascribed to the intrinsic flexoelectricity induced by strain gradient at domain walls.

Based on the inherent photoactivity of BVO, the emerging polarization at domain wall implies the feasibility of the flexo-phototronic effect in our system. We further explore such a flexo-phototronic behavior by conducting RhB degradation experiments since dye degradation reaction could be driven by either solar energy or mechanical vibrational energy for photoactive semiconductors with piezoresponse [36] (inset in Fig. 1f). In this experiment, the absorption of RhB by catalyst is neglectable based on the controlled dark condition without any stimuli (green line in Fig. 1f). Surprisingly, although monoclinic space group (i.e., I_2/b) of BVO is centro-symmetric, we observed an outstanding flexo-degradation performance, which is even much higher than its photo-degradation activity in the thin film structure. Significantly, the rate constant (k) of flexo-photo-degradation is ~10 folds higher than that of photo-degradation effect, as shown in Fig. S3 and Table S1. Considering that the piezo-phototronic effect only occurs in piezoelectric materials, this unprecedented result inspires us to further investigate the flexo-phototronic mechanism of driving piezoresponse in centro-symmetric BVO and the critical role of domain patterns.

3.2. Effect of flexoelectricity on the photoelectrochemistry of BVO

To examine the flexo-phototronic effect, we first consider it as a combination of flexo-degradation and photo-degradation processes. In Fig. 2a, the photo-degradation effect mainly occurs inside BVO film, including absorption of light, generation of photocarriers and transport of photocarriers [37]. The band diagram of BVO was identified in Fig. S4. On the other hand, the flexo-degradation course relies on tuning surface screen charges. With antiparallel in-plane flexopotential at domain walls, the projected flexopotential is from A to B domains in each bundle domain. It could be anticipated that the intrinsic in-plane flexopotential can enhance the photo-catalytic efficiency of BVO. As illustrated in Fig. 2b, under light illumination, radicals generated from majority of charge carriers (i.e., electrons in n-type BVO) can reduce $HAuCl_4$ to produced Au on surface. Therefore, the deposition of Au nanoparticles would be prominent in the electron-rich domain. As

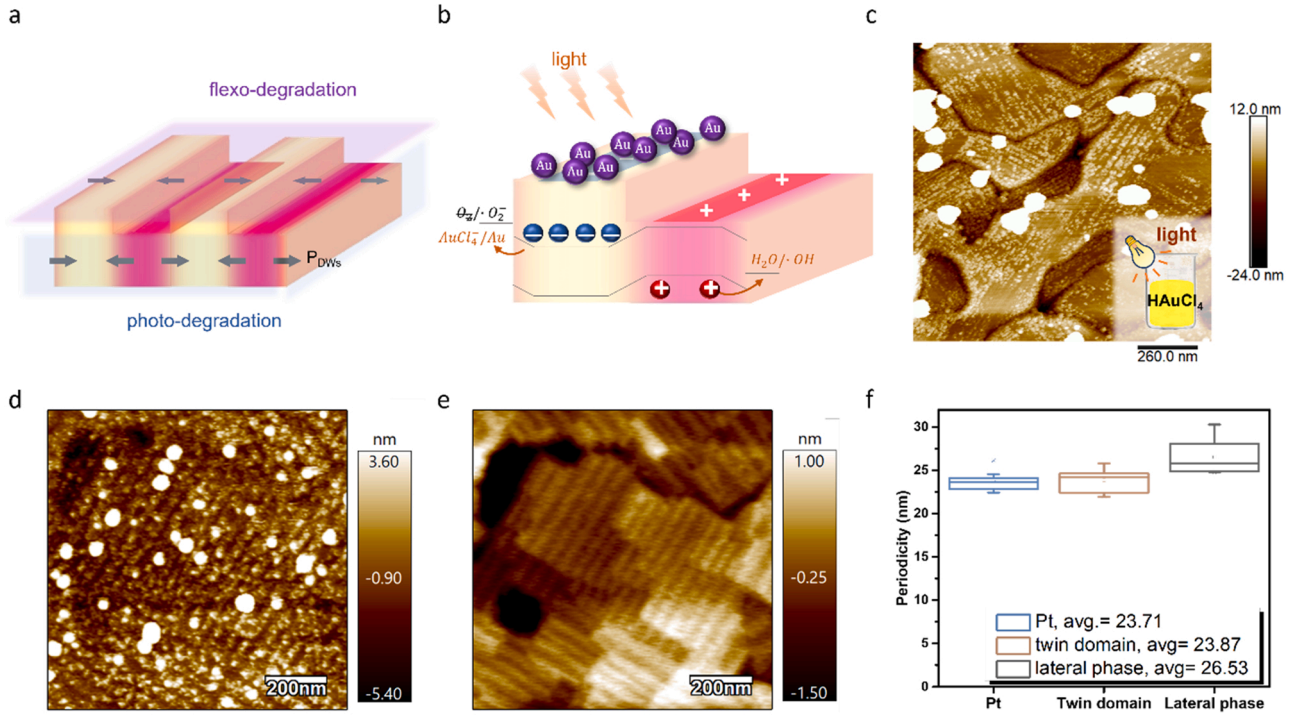

Fig. 2. (a) Schematic illustration of flexo-degradation and photo-degradation processes on BVO/YSZ. The projected flexopotential is from A to B domains in each bundle domain. (b) Plausible mechanism of photo-catalytic effect. The flexopotential leads to the effectively separation of photo-generated carriers and the screen charges on surface. (c, d) AFM image of BVO/YSZ after photo-reduction of $HAuCl_4$. (e) Surface at the same area with (d) after cleaning. (f) Periodicity of (d, e) and phase channel (Fig. S5c) calculated by FFT. AFM surface after photoreduction was collected by tapping mode scanning while the clean surface was obtained by contact mode following, which could effectively remove Au nanoparticles.

highlighted in Fig. 2c, the deposition of Au nanoparticles from photo-reduction reaction indeed shows domain selectivity on BVO surface. It demonstrates that with flexopotential, the majority charge carriers (i.e., electrons) would consequently penetrate through domain wall and concentrate at B domains to dominate the photo-reduction reaction, whereas the minority charge carriers (i.e., holes) concentrate at A domains and show incapability for $HAuCl_4$ reduction. The significant role of domain walls in the photo-reduction of $HAuCl_4$ can be examined by analyzing the periodicity of the deposited Au nanoparticles. Compared with surface after the photodeposition (Fig. 2d) and further cleaned surface at the same area (Fig. 2e), the periodicity could be obtained by mathematical method of Fast Fourier Transform (FFT). As revealed in Fig. 2f, the periodicity and pattern of the deposited Au nanoparticles are morphologically consistent with domain width (Fig. 2e) and the corresponding in-plane PFM signal (Fig. S5c), confirming that Au nanoparticles prefer to deposit at the areas of upper domains (B domain). With the increase of deposition time, instead of thoroughly covering the BVO surface, additional deposited Au nanoparticles tend to nucleate on the pre-formed nanoparticles. This observation suggests an effective electron transfer pathway from active B domains to the pre-formed Au nanoparticles (Fig. S6). All the AFM images were taken after rinsing the samples. The observed well-defined microstructural features suggest a strong connection between BVO/YSZ and Au. It is also worth noting that other possible driving force such as a work function difference between the {001} and the {101}/{011} facets of BVO also promotes photo-generated electron to concentrate at {001} facet [38,39], enhancing the Au deposition on surface of BVO/YSZ with {001} facet.

3.3. *Flexo-catalytic and flexo-phototronic mechanism of BVO/YSZ thin film*

In order to prove the flexo-catalytic feature on BVO, $HAuCl_4$ was introduced to conduct the flexo-deposition of Au nanoparticles on BVO. In the absence of reducing reagent and light illumination, $HAuCl_4$ can be reduced to Au nanoparticles (Fig. 3a) by reacting with radicals from flexo-catalytic mechanism (discussed in the next paragraph) [40]. Such a feature can be further corroborated by conducting the same Au deposition experiment on pure YSZ substrate, in which Au nanoparticles were barely produced (Fig. S6).

In the flexo-catalytic mechanism, the flexopotential is balanced by screen charges on the surface of twin domains, as illustrated in Fig. 3b. Due to the head-to-head polarization distribution, screen charges, i.e., e^- and h^+, would accumulate on A and B domain area respectively. (The calculated flexoelectrically induced open-circuit voltage across each domain wall is ~ 0.25 mV. See details in supplementary text S2.) In addition, ultrasonic vibration plays a significant role by creating a sinusoid function of hydraulic pressure, i.e., stress in aqueous solution (Fig. 3c). Subsequently, the localized strain gradient and flexopotential at domain wall would also fluctuate with time to redistribute and release the screen charges from surface (e.g., the process from P_1 to P_2 and P_3 is displayed by the dynamic evolution from Fig. 3d to 3e and 3f). As a consequence, the extra charges would spread into solution and serve as active charges (Fig. 3e, f, and see details in Fig. S7). These free charge carriers further react with water and the dissolved oxygen, producing reactive oxygen species, e.g., •OH or $•O_2^-$ radicals, for participation in the RhB degradation reaction [41]. To identify the reactive oxygen species responsible for flexo-degradation reaction, the production of radicals is verified by the electron paramagnetic resonance (EPR) technique using 5,5-dimethyl-1-pyrroline N-oxide (DMPO) and dimethyl sulfoxide (DMSO) as spin scavenger. In Fig. 3g and 3h, the resonance peaks of DMPO-•OH were detected, showing that •OH radicals were the main reactive species. The results show that the EPR intensity of superoxide radicals ($\cdot O^-_2$) is neglectable (Fig. 3i, j) compared to the intensity of hydroxyl radicals (·OH) (Fig. 3g, h). This means that hydroxyl radicals are the main free radicals for both flexo-degradation and flexo-photo-degradation due to the anaerobic condition in

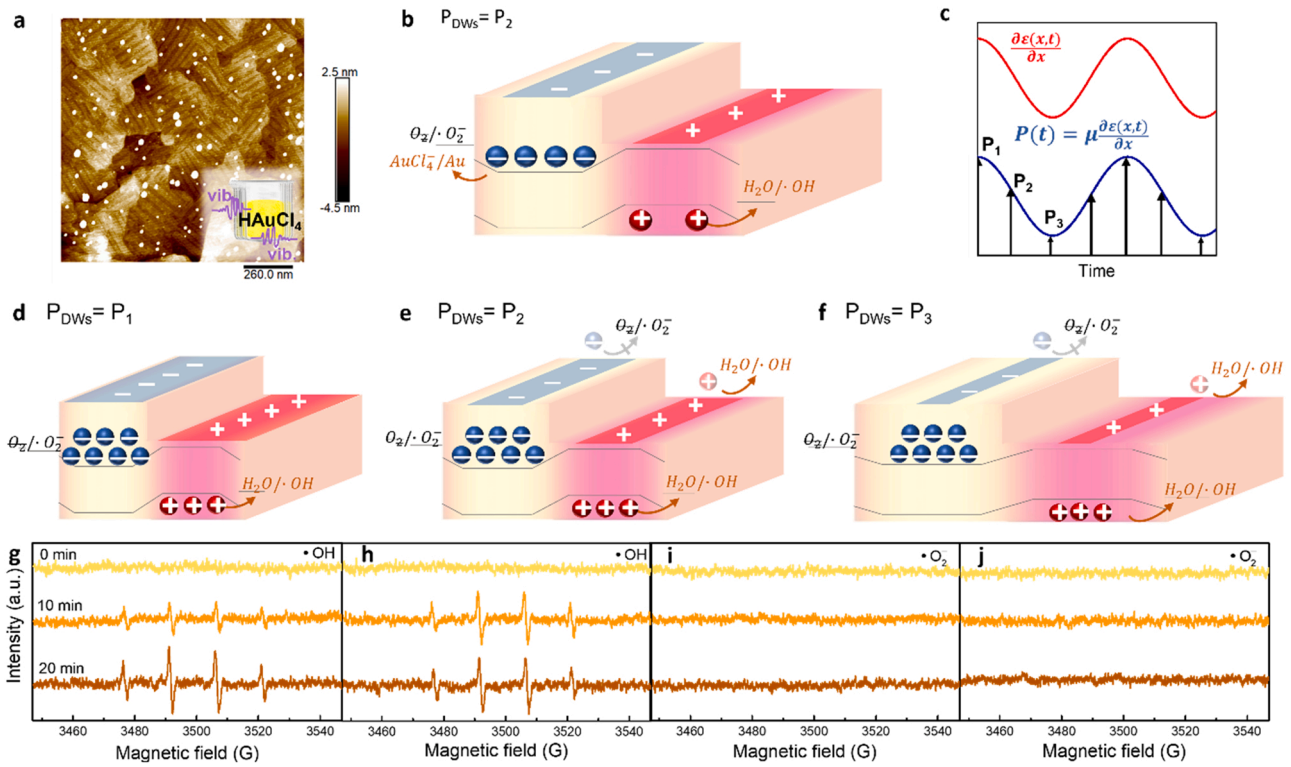

Fig. 3. (a) BVO/YSZ surface after flexo-catalytics. (b) Schematic illustration of flexo-catalytics when $P_{DWs} = P_2$. (c) The strain gradient and resultant flexopotential under ultrasonic vibration with time dependence. The black arrows represent the instant polarization with vibration stimuli. (d, e, f) Schematic illustration of flexo-phototronic effect during P_{DWs} from P_1 to P_2 and P_3. (g, h) EPR spectra of DMPO-•OH over BVO film in aqueous dispersion with vibration stimuli under dark condition and vibration stimuli under light illumination. (i, j) EPR spectra of DMSO-$•O_2^-$ over BVO film in aqueous dispersion with vibration stimuli under dark condition and vibration stimuli under light illumination.

aqueous condition [42]. Therefore, under darkness condition with vibration (i.e., flexo-degradation in Fig. 3g), •OH radicals could be generated by mechanical vibration and the concentration increases with vibration time. On the other hand, considering the flexo-phototronic effect under light illumination, due to the nature of n-type semiconductor in BVO, the photo-electrons and photo-voltage would compete with the flexoelectric field on domain walls, determining the screening charge, which is •OH radical as well. The concentration of •OH radicals was further enhanced since the photo-generated holes participate the degradation while the agitation and ultrasonic vibration facilitate the creation of radicals. In addition, we have collected the EPR spectra of •OH for the BVO sample under light illumination without ultrasonic vibration. As shown in Fig. S8, only background noise was recorded within 20 mins. This outcome was consistent with the result of photo-degradation shown in Fig. 1f, in which nearly negligible activity of photo-degradation was observed within 20 min of reaction. This phenomenon can be understood by the limited light absorption ability of BVO as a result of the low film thickness (200 nm).

Other factors such as degree of inhomogeneity (i.e., density of domain walls and thickness dependence) and flexo-degradation activity of BVO without twin domains is discussed in Fig. S9, 10, and 11. Besides, as illustrated in Fig. S12, the internal electric field is modulated by external ultrasonic vibration. Similar to the photoelectrochemical application on BVO [43,44], the temporary bending of band structure can promote carrier transfer and reduce the trapping of carriers not only at the interface but also inside the thin film because the flexoelectric potential exists throughout the thin film at domain walls. This results in the higher rate constant of flexo-photo degradation than the sum of flexo- and photo-degradation (Table S1), which highly emphasizes the coupling effect between photo-degradation and flexo-degradation at domain walls, showing that the ultrasonic vibration not only modulates the screen charges for radical generation, but also tilts the conduction band, enhancing the potential of flexo-phototronic property, which accounts for the dramatic flexo-photodegradation effect with 10-time higher rate constant than photo-degradation of RhB degradation.

3.4. Photoconductivity of flexoelectric BVO/YSZ thin film

Since the electric field in domain walls induced by ferroelastic domains can promote separation of photocarriers for enhancing photochemical reactivity [45], the implication of BVO ferroelastic domain pattern can be realized by building up the close relationship between the domain pattern and the photoelectrochemical effect. In this experiment, conductive AFM tips were used to simultaneously detect the morphology and current distribution. As illustrated in Fig. 4a, the circuit was formed by using AFM tip to detect the current from the sample surface to the top electrode, which is the direct method to record the distribution of photocarrier in the domain configuration, demonstrated in Fig. 4d. Unlike the topography image (Fig. 4b) and the conductivity pattern at dark condition (Fig. 4c), the specific stripe-like domains display higher photocurrent with the same periodicity in PFM in-plane phase signal (Fig. 4e). In other words, the photocarriers can be extracted and collected at specific domains (i.e., the B domains) under light illumination. Since the flexoelectric effect results from inhomogeneity in ferroelastic twin domain walls, the distribution of polar domain walls is exact every twin domain wall in morphology. Thus, the head-to-head direction of neighboring flexopotential at domain walls could facilitate photo-carriers separation and further collected at upper domains (B domains) in morphology. This outcome delivers the critical evidence that the flexopotential at domain walls can dominate the transportation and separation of photocarriers in BVO because light harvesting efficiency (i.e., optical bandgap) of BVO remains the same regardless of the presence of domain walls (Fig. 4f). In addition, it is important to note here that the diffusion length of electron and holes in BVO are

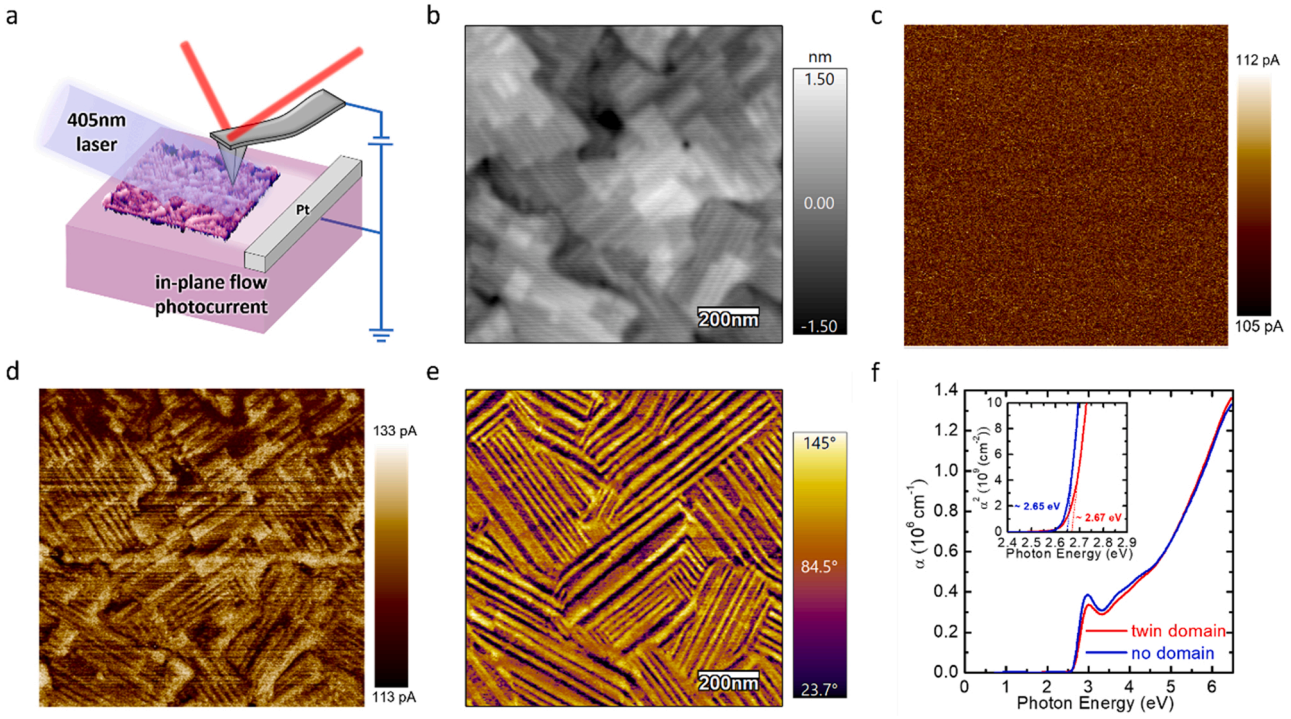

Fig. 4. (a) Schematic diagram of the experimental setup and the in-plane photo-current flow generated by 405 nm point laser. A platinum electrode was constructed on the BVO/YSZ surface. (b) Topography, and (c) dark current acquired at 8 V sample bias. (d) Photo-current acquired at 8 V sample bias. (e) The corresponding PFM in-plane phase signal at 1.5 V_{ac}. (f) The optical property of BVO samples with twin domains and without twin domains. The bandgap is almost identical, revealing the absorption activity is also identical. The morphology of BVO samples with twin domains and without twin domains is in Fig. S11.

70–200 nm [46–49], which is ~ three-folds larger than the twin domain width. This feature makes the effective separation of photo-generated electrons by the inherent electric field, which accounts for the observed flexo-phototronics effect as wall.

Furthermore, another ferroelastic material (i.e., γ-WO_3) is conducted to demonstrate that the flexoelectricity and flexo-degradation is a general phenomenon in twin domain walls. γ-WO_3 is also a centrosymmetric system and it is experimentally revealed with polar domain walls recently [50]. With evidence, it is demonstrated as flexo-degradation catalyst as well in this study (Fig. S13). This extraordinary phenomenon opens new avenue to the development of flexo-phototronics with non-polar systems using material inhomogeneity. Based on this concept, we expect that in other photo-active semiconductors with inhomogeneities at atomic scale, flexo-phototronics effect could be triggered regardless of the symmetry of the crystal structure and material category (e.g., epitaxial thin film or polycrystalline ceramics).

4. Conclusions

All in all, this study illustrates the engineering application of multifunctional topological defects and opens up opportunities for exploiting the flexo-phototronic effect based on centro-symmetric material. Ferroelastic twin domain feature of BVO was predicted by DFT calculations and confirmed by PFM. Based on the mesoscopic evidence of selective photodeposition of Au nanoparticles on twin domains as well as macroscopic evidence of the giant improvement in reaction rate constant of flexo-photo-degradation, the flexopotential not only serves as a pathway for photogenerated carriers to accumulate at specific domain area under light illumination, but also holds promising engineering potentials for converting mechanical vibrational energy to chemical energy for photoelectrochemical applications. Our results demonstrate the predominant role of strain gradients at domain walls by flexoelectricity, and the localized flexopotential can be combined with the inherent photoactivity, lessening the gap for engineering the flexo-phototronic effect in centrosymmetric materials.

CRediT authorship contribution statement

Pao-Wen Shao: Conceptualization, Methodology, Formal analysis, Validation, Data Curation. Writing - Original Draft. **Meng-Chin Lin**: Validation, Investigation. **Qian Zhuang**: Validation, Software. **Jiawei Huang**: Validation, Software. **Shi Liu**: Supervision. **Hsiao-Wen Chen**: Validation, Data Curation. **Hsiang-Lin Liu**: Funding acquisition, Supervision. **Yu-Jung Lu**: Supervision, Funding acquisition. **Yung-Jung Hsu:** Supervision. **Jyh-Ming Wu**: Supervision. **Yi-Chun Chen**: Supervision. **Ying Hao Chu**: Writing - Review & Editing, Project administration, Funding acquisition, Supervision.

Declaration of Competing Interest

The authors declare that they have no known competing financial interests or personal relationships that could have appeared to influence the work reported in this paper.

Acknowledgments

This work is supported by Ministry of Science and Technology, Taiwan (grant No. MOST 109-2124-M-009-009-, MOST 109-2124-M-009-001-MY3, MOST 109-2634-F-009-028, MOST 106-2112-M-001-036-MY3, MOST 109-2112-M-001-043-MY3) and the Center for Emergent Functional Matter Science of National Chiao Tung University from The Featured Areas Research Center Program within the framework of the Higher Education Sprout Project by the Ministry of Education (MOE) in Taiwan. H.-L. L. acknowledgments the support from Ministry of Science and Technology, Taiwan under grant number MOST 108-2112-M-003-013. Z. Q., J. H. and S. L. acknowledges the support from Westlake Education Foundation and the computational resource from Westlake University HPC Center. Y.-J. L. acknowledges the support from

Academia Sinica (AS-CDA-108-M08).

Appendix A. Supporting information

Supplementary data associated with this article can be found in the online version at doi:10.1016/j.apcatb.2022.121367.

References

[1] E.Y. Tsymbal, E.R.A. Dagotto, C.B. Eom, R. Ramesh, Multifunctional Oxide Heterostructures, OUP Oxford, 2012.
[2] Y.-L. Liu, J.M. Wu, Synergistically catalytic activities of $BiFeO_3/TiO_2$ core-shell nanocomposites for degradation of organic dye molecule through piezophototronic effect, Nano Energy 56 (2019) 74–81.
[3] L. Zhu, Z.L. Wang, Recent progress in piezo-phototronic effect enhanced solar cells, Adv. Funct. Mater. 29 (2019), 1808214.
[4] C. Pan, M. Chen, R. Yu, Q. Yang, Y. Hu, Y. Zhang, Z.L. Wang, Progress in piezo-phototronic-effect-enhanced light-emitting diodes and pressure imaging, Adv. Mater. 28 (2016) 1535–1552.
[5] L. Pan, S. Sun, Y. Chen, P. Wang, J. Wang, X. Zhang, J.-J. Zou, Z.L. Wang, Advances in piezo-phototronic effect enhanced photocatalysis and photoelectrocatalysis, Adv. Energy Mater. 10 (2020), 2000214.
[6] X. Zhang, H. Wang, J. Zhang, J. Li, Z. Ma, J. Li, B. Leng, P. Niu, B. Liu, Enhanced optoelectronic performance of 3C–SiC/ZnO heterostructure photodetector based on Piezo-phototronic effect, Nano Energy 77 (2020), 105119.
[7] X. Wang, D. Peng, B. Huang, C. Pan, Z.L. Wang, Piezophotonic effect based on mechanoluminescent materials for advanced flexible optoelectronic applications, Nano Energy 55 (2019) 389–400.
[8] W. Wu, Z.L. Wang, Piezotronics and piezo-phototronics for adaptive electronics and optoelectronics, Nat. Rev. Mater. 1 (2016) 16031.
[9] G.F. Nataf, M. Guennou, J.M. Gregg, D. Meier, J. Hlinka, E.K.H. Salje, J. Kreisel, Domain-wall engineering and topological defects in ferroelectric and ferroelastic materials, Nat. Rev. Phys. 2 (2020) 634–648.
[10] E. Salje, H. Zhang, Domain boundary engineering, Phase Transit. 82 (2009) 452–469.
[11] J.F. Nye, P.P.L.J.F. Nye, Physical Properties of Crystals: Their Representation by Tensors and Matrices, Clarendon Press, 1985. https://books.google.com.tw/books?id=ugwql-uVB44C.
[12] H. Yokota, N. Hasegawa, M. Glazer, E.K.H. Salje, Y. Uesu, Direct evidence of polar ferroelastic domain boundaries in semiconductor $BiVO_4$, Appl. Phys. Lett. 116 (2020), 232901.
[13] L. Zhang, D. Chen, X. Jiao, Monoclinic structured $BiVO_4$ nanosheets: hydrothermal preparation, formation mechanism, and coloristic and photocatalytic properties, J. Phys. Chem. B 110 (2006) 2668–2673.
[14] J. Su, L. Guo, N. Bao, C.A. Grimes, Nanostructured $WO_3/BiVO_4$ heterojunction films for efficient photoelectrochemical water splitting, Nano Lett. 11 (2011) 1928–1933.
[15] P.M. Rao, L. Cai, C. Liu, I.S. Cho, C.H. Lee, J.M. Weisse, P. Yang, X. Zheng, Simultaneously efficient light absorption and charge separation in $WO_3/BiVO_4$ core/shell nanowire photoanode for photoelectrochemical water oxidation, Nano Lett. 14 (2014) 1099–1105.
[16] R. Munprom, P.A. Salvador, G.S. Rohrer, Polar domains at the surface of centrosymmetric $BiVO_4$, Chem. Mater. 26 (2014) 2774–2776.
[17] S. Van Aert, S. Turner, R. Delville, D. Schryvers, G. Van Tendeloo, E.K.H. Salje, Direct observation of ferrielectricity at ferroelastic domain boundaries in CaTiO3 by electron microscopy, Adv. Mater. 24 (2012) 523–527.
[18] X. Liu, F. Zhang, P. Long, T. Lu, H. Zeng, Y. Liu, R.L. Withers, Y. Li, Z. Yi, Anomalous photovoltaic effect in centrosymmetric ferroelastic $BiVO_4$, Adv. Mater. 30 (2018), 1801619.
[19] X. Xue, W. Zang, P. Deng, Q. Wang, L. Xing, Y. Zhang, Z.L. Wang, Piezo-potential enhanced photocatalytic degradation of organic dye using ZnO nanowires, Nano Energy 13 (2015) 414–422.
[20] J. Nie, Y. Zhang, L. Li, J. Wang, Piezo-phototronic effect enhanced photodetectors based on MAPbI3 perovskite, J. Mater. Chem. C 8 (2020) 2709–2718.
[21] Y.-L. Huang, H.-J. Liu, C.-H. Ma, P. Yu, Y.-H. Chu, J.-C. Yang, Pulsed laser deposition of complex oxide heteroepitaxy, Chin. J. Phys. 60 (2019) 481–501.
[22] Y. Chen, X. Ma, D. Li, H. Wang, C. Huang, Mechanism of enhancing visible-light photocatalytic activity of $BiVO_4$ via hybridization of graphene based on a first-principles study, RSC Adv. 7 (2017) 4395–4401.
[23] P. Giannozzi, S. Baroni, N. Bonini, M. Calandra, R. Car, C. Cavazzoni, D. Ceresoli, G.L. Chiarotti, M. Cococcioni, I. Dabo, A. Dal Corso, S. de Gironcoli, S. Fabris, G. Fratesi, R. Gebauer, U. Gerstmann, C. Gougoussis, A. Kokalj, M. Lazzeri, L. Martin-Samos, N. Marzari, F. Mauri, R. Mazzarello, S. Paolini, A. Pasquarello, L. Paulatto, C. Sbraccia, S. Scandolo, G. Sclauzero, A.P. Seitsonen, A. Smogunov, P. Umari, R.M. Wentzcovitch, QUANTUM ESPRESSO: a modular and open-source software project for quantum simulations of materials, J. Phys. Condens. Matter 21 (2009), 395502.
[24] K.F. Garrity, J.W. Bennett, K.M. Rabe, D. Vanderbilt, Pseudopotentials for high-throughput DFT calculations, Comput. Mater. Sci. 81 (2014) 446–452.
[25] B. Meyer, D. Vanderbilt, Ab initio study of ferroelectric domain walls in $PbTiO_3$, Phys. Rev. B 65 (2002), 104111.
[26] T.H. Yeom, S.H. Choh, K.J. Song, M.S. Jang, The domain structure of ferroelastic $BiVO_4$ studied by magnetic resonances, J. Phys. Condens. Matter 6 (1994) 383–392.
[27] S.H. Choh, M.S. Jang, Domain structure and magnetic resonance studies of ferroelastic $BiVO_4$ revisited, Mater. Res. Express 3 (2016), 045021.
[28] L. Goncalves-Ferreira, S. Redfern, E. Artacho, E. Salje, Ferrielectric twin walls in $CaTiO_3$, Phys. Rev. Lett. 101 (2008), 097602.
[29] H. Yokota, H. Usami, R. Haumont, P. Hicher, J. Kaneshiro, E.K.H. Salje, Y. Uesu, Direct evidence of polar nature of ferroelastic twin boundaries in $CaTiO_3$ obtained by second harmonic generation microscope, Phys. Rev. B 89 (2014), 144109.
[30] H. Yokota, S. Matsumoto, E.K.H. Salje, Y. Uesu, Symmetry and three-dimensional anisotropy of polar domain boundaries observed in ferroelastic $LaAlO_3$ in the complete absence of ferroelectric instability, Phys. Rev. B 98 (2018), 104105.
[31] A. Gruverman, S.V. Kalinin, Piezoresponse force microscopy and recent advances in nanoscale studies of ferroelectrics, J. Mater. Sci. 41 (2006) 107–116.
[32] A. Gruverman, M. Alexe, D. Meier, Piezoresponse force microscopy and nanoferroic phenomena, Nat. Commun. 10 (2019) 1661.
[33] A. Abdollahi, N. Domingo, I. Arias, G. Catalan, Converse flexoelectricity yields large piezoresponse force microscopy signals in non-piezoelectric materials, Nat. Commun. 10 (2019) 1266.
[34] W. Zhang, D. Yan, X. Tong, M. Liu, Ultrathin lutetium oxide film as an epitaxial hole-blocking layer for crystalline bismuth vanadate water splitting photoanodes, Adv. Funct. Mater. 28 (2018), 1705512.
[35] B.J. Rodriguez, R.J. Nemanich, A. Kingon, A. Gruverman, S.V. Kalinin, K. Terabe, X.Y. Liu, K. Kitamura, Domain growth kinetics in lithium niobate single crystals studied by piezoresponse force microscopy, Appl. Phys. Lett. 86 (2005), 012906.
[36] S. Li, Z. Zhao, J. Zhao, Z. Zhang, X. Li, J. Zhang, Recent advances of ferro-, piezo-, and pyroelectric nanomaterials for catalytic applications, ACS Appl. Nano Mater. 3 (2020) 1063–1079.
[37] Y. Ma, S.R. Pendlebury, A. Reynal, F. Le Formal, J.R. Durrant, Dynamics of photogenerated holes in undoped $BiVO_4$ photoanodes for solar water oxidation, Chem. Sci. 5 (2014) 2964–2973.
[38] G.-L. Li, First-principles investigation of the surface properties of fergusonite-type monoclinic $BiVO_4$ photocatalyst, RSC Adv. 7 (2017) 9130–9140.
[39] R. Li, F. Zhang, D. Wang, J. Yang, M. Li, J. Zhu, X. Zhou, H. Han, C. Li, Spatial separation of photogenerated electrons and holes among {010} and {110} crystal facets of $BiVO_4$, Nat. Commun. 4 (2013) 1432.
[40] L.M. Frias Batista, V.K. Meader, K. Romero, K. Kunzler, F. Kabir, A. Bullock, K. M. Tibbetts, Kinetic control of $[AuCl_4]-$ photochemical reduction and gold nanoparticle size with hydroxyl radical scavengers, J. Phys. Chem. B 123 (2019) 7204–7213.
[41] Y. Wang, X. Wen, Y. Jia, M. Huang, F. Wang, X. Zhang, Y. Bai, G. Yuan, Y. Wang, Piezo-catalysis for nondestructive tooth whitening, Nat. Commun. 11 (2020) 1328.
[42] X. Xu, Y. Sun, Z. Fan, D. Zhao, S. Xiong, B. Zhang, S. Zhou, G. Liu, Mechanisms for·O2- and·OH production on flowerlike $BiVO_4$ photocatalysis based on electron spin resonance, Front. Chem. 6 (2018).
[43] M.A. Gaikwad, U.P. Suryawanshi, U.V. Ghorpade, J.S. Jang, M.P. Suryawanshi, J. H. Kim, Emerging Surface, Bulk, and Interface Engineering Strategies on BiVO4 for Photoelectrochemical Water Splitting, Small, n/a 2105084.
[44] W. Dong, Y. Guo, Y. Zhang, H. Li, H. Liu, Photoelectric properties of BiVO4 thin films deposited on fluorine doped tin oxide substrates by a modified chemical solution deposition process, Int. J. Hydrog. Energy 39 (2014) 5569–5574.
[45] R. Munprom, P.A. Salvador, G.S. Rohrer, Ferroelastic domains improve photochemical reactivity: a comparative study of monoclinic and tetragonal (Bi1−0.5xNa0.5x)(V1−xMox)O4 ceramics, J. Mater. Chem. A 4 (2016) 2951–2959.
[46] A.J.E. Rettie, H.C. Lee, L.G. Marshall, J.-F. Lin, C. Capan, J. Lindemuth, J. S. McCloy, J. Zhou, A.J. Bard, C.B. Mullins, Combined charge carrier transport and photoelectrochemical characterization of $BiVO_4$ single crystals: intrinsic behavior of a complex metal oxide, J. Am. Chem. Soc. 135 (2013) 11389–11396.
[47] F.F. Abdi, T.J. Savenije, M.M. May, B. Dam, R. van de Krol, The origin of slow carrier transport in $BiVO_4$ thin film photoanodes: a time-resolved microwave conductivity study, J. Phys. Chem. Lett. 4 (2013) 2752–2757.
[48] J. Song, M.J. Seo, T.H. Lee, Y.-R. Jo, J. Lee, T.L. Kim, S.-Y. Kim, S.-M. Kim, S. Y. Jeong, H. An, S. Kim, B.H. Lee, D. Lee, H.W. Jang, B.-J. Kim, S. Lee, Tailoring crystallographic orientations to substantially enhance charge separation efficiency in anisotropic $BiVO_4$ photoanodes, ACS Catal. 8 (2018) 5952–5962.
[49] D.K. Zhong, S. Choi, D.R. Gamelin, Near-complete suppression of surface recombination in solar photoelectrolysis by "Co-Pi" catalyst-modified W:$BiVO_4$, J. Am. Chem. Soc. 133 (2011) 18370–18377.
[50] S. Yun, K. Song, K. Chu, S.-Y. Hwang, G.-Y. Kim, J. Seo, C.-S. Woo, S.-Y. Choi, C.-H. Yang, Flexopiezoelectricity at ferroelastic domain walls in WO_3 films, Nat. Commun. 11 (2020) 4898.